Research Paper   Open Access

Power Grid Reliability Improvement through Forecasting with Complex-Valued Neural Networks under System Contingency

Mahdi Motalleb[1], Sasidharan Sreedharan[1], Hossein Sangrody[2],
Alireza Eshraghi[3], Reza Ghorbani[1]

1-University of Hawaii at Manoa, Hawaii, Email: {motalleb, sasi, rezag}@hawaii.edu
2-State University of New York at Binghamton, Email:habdoll1@binghamton.edu
3-University of California, San Diego, Email: seshragh@ucsd.edu

ABSTRACT: *To increase the reliability of power system, network should have the most efficient reaction against contingencies. This efficient response makes the grid self-healing. Estimating the network state in the contingencies requires a relatively accurate forecasting variables of the grid. This paper describes a heuristic method to forecast voltage amplitudes and angles in the abnormal situations. This approach combines multi-stage learning of Complex-Valued Neural Networks (CVNN) and Time Domain Power Flow (TDPF). After ensuring the accuracy of forecasting, different scenarios are applied to model to simulate various contingencies. Next, the sensitive grid buses are detected using the heuristic method, thus the network can be adapted to cope with the contingencies reliably. Adapting the network means changing power injections at load or generation buses in order to have the best reaction against the contingency. Utilizing the proposed method not only increases the grid reliability, but also reduces the enormous mathematical calculations of power flow in the abnormal situations. Also, the proposed method is used to find the optimal location and size of the batteries for contingency management and frequency regulation. The innovative approach is verified by applying to a real-world model of an island (Maui Island in Hawaii, United States).*
Index Terms*: Complex-Valued Neural Networks (CVNN), Time Domain Power Flow (TDPF), Forecasting, Contingency, Reliability.*

I.   Introduction

An important problem in power grid is less quality of power delivery in abnormal situations. In order to have a reliable reaction by the grid in the contingencies, the power grid variables should be predicted accurately. In the field of power grid, forecasting has been started theoretically since decades. Power systems experts have utilized different mathematical and statistical techniques in order to forecast the grid variables such as load, voltage, power losses, demand, and renewable generations [1]. Power flow contains four groups of parameters including voltage amplitudes, voltage angles, active powers, and reactive powers. The focus of this paper is to forecast the two first parameters. The network adapts to the contingencies utilizing the predicated values. This means that the network efficiently and reliably copes with the abnormal situations. The following subsections contain a literature review and contribution of this study.

A. Literature Review

In literature review three different items can be considered: forecasting parameters, forecasting purposes, and forecasting techniques.Some of the forecast parameters are related to power flow. Different methods were utilized to forecast short-term and day ahead power flow parameters [2, 3]. Another forecasting parameter is load which Bing et al: [4] proposed a controlling strategy for voltage and reactive power optimization based on load forecasting. Renewable generation is another forecasting parameter. Liu et al: [5] proposed a method to control the grid voltage using wind generation forecasting. The purposes of [4] and [5] were to control various parameters of the grid using forecasting. Another useful purpose of the forecasting is to make good decisions in marketing area. Zhou et al: applied wind forecasting to electricity markets [6]. In addition, forecasting can be used in unit commitment and economic

dispatch in the power grids [7]. Dragomir [8] defined a frame work for load forecasting in low voltage grids with distributed power generation from renewable energy resources. Hoiles [9] worked on nonparametric forecasting demand to increase the grid reliability based on Afriats theorem. Heins et al: [10] proposed a method to determine the grid states based on estimating the vector of active and reactive power through voltage magnitude and angle measurements using Kalman filter. Many studies were completed in order to forecast the grid parameters including: electricity price [11], wind generations [12-14], photo-voltaic generations [15], etc.

To solve the forecasting problems in the power systems, computational and intelligent techniques have been widely used, such as Artificial Neural Networks (ANN) [11, 12, 14-17], fuzzy-logic approach [18], and genetic algorithm [19]. Anbazhagan [11] performed price forecasting for day-ahead using recurrent neural networks. A model for wind forecasting was proposed by Aquino et al., based on ANN [12]. A combination of load and wind power forecasting was carried out by Quan et al: through neural network-based prediction intervals [14]. Yona et al. [15] determined a method for insolation prediction with fuzzy and then they added ANN for long term ahead corrected prediction of photo-voltaic outputs. Kurbatsky et al: [16] applied two stages of adaptive neural network to have a short-time forecast of power system parameters. Lee worked on ensemble forecasting the short-term wind power through Gaussian processes and ANN [17]. Saez et al. [20] developed a fuzzy prediction interval model for a microgrid in order to forecast renewable resources and loads.

B. Contributions of the Heuristic Method

In the power grid, contingencies (e.g., losing a generator) change the voltage amplitudes and angles. In this paper, forecasting these two parameters has been performed for the purpose of the contingency analysis. Additionally, in this study, the utilized forecasting tool is Complex-Valued Neural Networks (CVNN) which has been used in literature for contingency management [21].In this study, at first, CVNN is applied to the processed data which is a combination of actual load values and output calculations of Time Domain Power Flow (TDPF). The learning part of CVNN includes two stages: the first stage is through voltage amplitudes and reactive powers and the second is through voltage angles and active powers. This multi-stage learning makes the grid smarter in order to have more reliable operation. Next, various contingencies are applied to the grid and sensitive buses (generations or loads) for detection. Finally, the network adapts to the contingencies with a higher reliability and lower power interruption.

In addition, the proposed method finds the optimal placing and capacity of storage system for contingency management and coping with the contingencies to regulate the grid frequency and voltage.Two case studies are modeled in this paper: one is IEEE 14-bus model and another is model of an Island (Maui Island in Hawaii, United States) including 184 buses. Various scenarios as contingencies are applied to both case studies and the forecast and actual values are compared to demonstrate the high accuracy of the proposed method. These contingencies are: loss the generations, faults or loss the lines, and suddenly or slowly changing of wind generations. In the second case study, the optimal place and size of storage system has been obtained.

II. Newton Raphson Time-Domain PowerFlow

The power flow problem can mathematically be defined as:

$$[I_{Bus}] = [Y_{Bus}][V_{Bus}]$$

(1)

where I_{Bus} is injected current to the buses which is positive in generation buses (PV-buses and slack bus) and is negative in loads (PQ-buses). Y_{Bus} is admittance matrix of the grid and V_{Bus} is voltage of the buses. The Newton-Raphson technique is used to solve the power flow equations [22]. For each bus k, $I_k = \sum_{i=1}^{n} y_{ki}.v_i$, which n is the number of the buses and y_{ki} is one array of Y_{Bus} matrix corresponding to bus i and k. For each bus k,

$$P_k + jQ_k = v_k I_k^*$$
(2)

where P_k, and Q_k are the active and reactive power entering to bus k (* is a complex conjugate and $j = \sqrt{-1}$).
Let,

$$v_k = V_k.e^{j\theta_k} = e_k + j.f_k$$
(3)

$$y_{ki} = Y_{ki}.e^{j\alpha_{ki}} = G_{ki} + j.B_{ki}$$
(4)

where $\theta_k = \tan^{-1}\dfrac{f_k}{e_k}$ and $\alpha_{ki} = \tan^{-1}\dfrac{B_{ki}}{G_{ki}}$. Using Equations (3) and (4) in (2):

$$P_k + jQ_k = V_k.e^{j\theta_k}\sum_{i=1}^{n}Y_{ki}e^{-j\alpha_{ki}}V_ie^{-j\theta_i}$$
(5)

Using Taylor series expansion, the final equation is:

$$\begin{bmatrix} \Delta P \\ \Delta Q \end{bmatrix} = \begin{bmatrix} \dfrac{\partial P}{\partial \theta} & \dfrac{\partial P}{\partial V}V \\ \dfrac{\partial Q}{\partial \theta} & \dfrac{\partial Q}{\partial V}V \end{bmatrix}\begin{bmatrix} \Delta \theta \\ \dfrac{\Delta V}{V} \end{bmatrix}$$
(6)

where the differential matrix is Jacobian. Numerical studies demonstrate that the changing of the voltage amplitudes and angles have negligible effect on the active and reactive power flows, respectively [22]. So Equation (6) can be rewritten as:

$$\begin{bmatrix} \Delta P \\ \Delta Q \end{bmatrix} = \begin{bmatrix} \dfrac{\partial P}{\partial \theta} & 0 \\ 0 & \dfrac{\partial Q}{\partial V}V \end{bmatrix}\begin{bmatrix} \Delta \theta \\ \dfrac{\Delta V}{V} \end{bmatrix}$$
(7)

Equation (7) clearly indicates multi-stage learning the system with CVNN. One stage is learning through the active powers and voltage angles and another one is learning through the reactive powers and voltage amplitudes.

In this paper, TDPF has been done with PSAT software in time domain where the grid's equipment are modeled dynamically. The purpose of time domain simulation is to solve the following problems in a typical time t and time step Δt:

$$f_n(x(t+\Delta t), y(t+\Delta t), f(t)) = 0$$
(8)

$$g(x(t+\Delta t), y(t+\Delta t)) = 0$$
(9)

where f and g are the algebraic and differential equations and function f_n is dependent on the method of integration. Equations (8) and (9) are nonlinear and solved through Newton-Raphson method. This method calculates the increments Δx^i and Δy^i of the state and algebraic variables and then updates the actual variables iteratively:

$$\begin{bmatrix} \Delta x^i \\ \Delta y^i \end{bmatrix} = -\begin{bmatrix} A_c^i \end{bmatrix}^{-1}\begin{bmatrix} f_n^i \\ g^i \end{bmatrix}$$
(10)

$$x^{i+1} = x^i + \Delta x^i$$
(11)

$$y^{i+1} = y^i + \Delta y^i$$
(12)

Where A_c^i is a matrix and dependents on the algebraic and state Jacobian matrices. x^{i+1} and y^{i+1} are the calculated values of x and y in time $t = i+1$, respectively [23]. The loop stops when the variable increment is less than a certain fixed tolerance or when iteration number reaches to its maximum value. There are two possible techniques to solve the above equations: Forward Euler Method and Trapezoidal Method, which the first is used in this study[23, 24].

By modeling the grid with TDPF, dynamic behaviors of the grid are analyzed and eigenvalues of the dynamic system can be controlled and adjusted. Additionally, the contingencies or disturbances can be easily applied to the model in various time intervals in order to analyze their effects on the grid [25, 26]. Thus, appropriate strategies can be adopted to have the most optimized reaction to overcome the contingency or fault. In this study, three different scenarios are applied to the model as the contingencies.

III. Complex-Valued Neural Networks

The major difference between ANN and CVNN is the nature of input parameters. Since real numbers are part of complex numbers, thus CVNN is counted as an extension of ANN. Fig. 1 demonstrates CVNN's architecture including input, hidden, and output layers. The input layer (X_m) includes two parts: input data (v) and previous output data (y). In this paper, in the first learning stage, v and y are the voltage amplitudes and reactive powers and in the second learning stage, v and y are the voltage angles and active powers, respectively. Weights (W) show the relationships between the nodes. If input vector, weights (i.e., $W_{n0}^1, W_{l0}^2, W_{nm}^1$, W_{ln}^2, etc.), and activations function (f_c) have real values, the network is normal ANN. Otherwise, the network is CVNN.
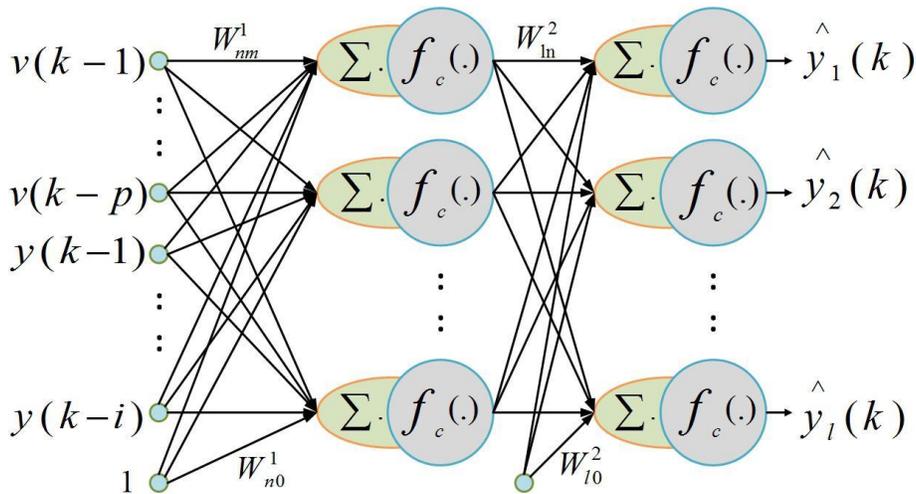

Fig. 1. Architecture of CVNN including the nodes, layers, and weights

Equation (13) shows the lth output of the network (forecast value):

$$\hat{y}_l(k) = f_c(W_{l0}^2 + \sum_n W_{ln}^2 H_n) \tag{13}$$

and the output of nth hidden neuron is given as:

$$H_n = f_c(W_{n0}^1 + \sum_m W_{nm}^1 X_m) \tag{14}$$

where $X_m = [v(k-1), v(k-2),..., v(k-p), y(k-1), y(k-2),..., y(k-i)]$, which includes m complex valued inputs ($m = i + p$). The whole values of m, n, i, l, and p are positive integers [27, 28]. In this study, the split sigmoid function is taken for the activation function as follows:

$$f_c(z) = \frac{1}{1+e^{-Re(z)}} + j\frac{1}{1+e^{-Im(z)}}, \tag{15}$$

where $z = x + jy$, with $j = \sqrt{-1}$. Using the split sigmoid function instead of non-split, avoids the problem of function's singularity. After applying complex back-propagation algorithm and calculation of the weight values (ΔW_{l0}^2, ΔW_{ln}^2, ΔW_{n0}^1, and ΔW_{nm}^1), the error is calculated using the following equation:

$$e_l(k) = y_l(k) - \hat{y}_l(k) \tag{16}$$

where $e_l(k)$ is the error between the lth actual output $y_l(k)$ and forecast output $\hat{y}_l(k)$ [28-30].
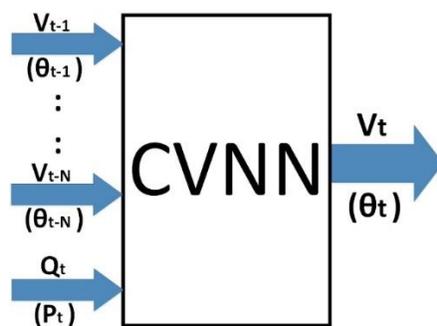
Fig. 2. Multi-stage learning of CVNN through the voltages and powers

IV. Methodology

This section describes the heuristic method to forecast the voltage amplitudes and angles, especially in the contingencies. This method includes a combination of TDPF and CVNN. The most important part of CVNN is learning through the available data. Next, performance of the learning is evaluated for calculations' validation. The proposed method and its application in the power grid, have been explained in this section.

A. Structure of CVNN in the proposed method

In the CVNN architecture, the number of neurons in input layer is:

$$m = B_n * (1 + NL) \tag{17}$$

where B_n is the number of the grid buses and NL is the number of previous outputs which are required to learn the network. NL is obtained using the following equation where res is resolution of real input data and Δt is time step of TDPF.

$$NL = \frac{res}{\Delta t} \tag{18}$$

In terms of the hidden layer, the number of neurons is obtained from an optimization to have the best trade-off between the forecast accuracy and calculations' speed. In this study, this number is 150 based on the trade-off results. The number of the output layer neurons is equal to the bus numbers (B_n). In the first and second learning stages, these outputs are the voltage amplitudes and angels, respectively.

B. Multi-stage learning of CVNN

Fig. 2 indicates two stages of learning with CVNN. The parameters at the top and bottom of the arrows are related to the first and second learning stages, respectively. The inputs of CVNN (in time t) include two parts: the first input is voltage amplitudes of last NL time series (including: $V_{t-1}, V_{t-2}, ..., V_{t-NL}$) and previous reactive power (Q_{t-1}), and the second one is voltage angles of last NL time series (including: $\theta_{t-1}, \theta_{t-2}, ..., \theta_{t-NL}$) and previous active power (P_{t-1}). The outputs of CVNN are forecast values of the voltage amplitudes and angles (V_t, θ_t). NL is the required number to learn the network. All of the mentioned parameters are vectors and have been defined for all buses. After learning, the proposed algorithm can predict the voltage amplitudes and angles in any requested time of

simulation (or times-ahead). To ensure that the forecast accuracy is enough, the forecast values are compared with actual data. These actual values have been obtained from TDPF.

C. The Proposed Forecast Algorithm with CVNN
        Block diagram of Fig. 3 shows the steps of forecasting through the proposed method which is a combination of CVNN and TDPF. The duty of TDPF is to create previous values of the voltage amplitudes and angles using active and reactive powers of the grid. CVNN uses these previous values to learn the system and to forecast the voltage amplitudes and angles. Two complex weight-vectors are generated by CVNN: W_{qv} is one of the learning weights through the voltage amplitudes (V) and reactive powers (Q) and $W_{p\theta}$ is another learning weight through the voltage angles (θ) and active powers (P). The actual data for active and reactive power (P, Q) are available for a whole day.
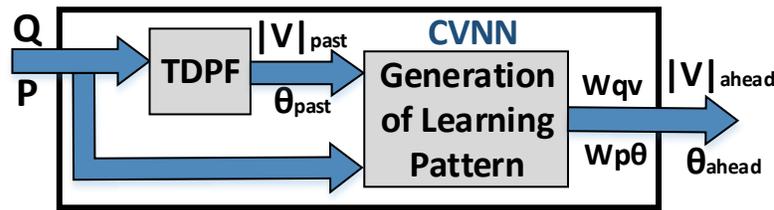

Fig. 3. Combination of CVNN and TDPF for forecasting

In order to prepare the parameters for CVNN, they should be transformed into complex domain. In this transformation, each angle of complex area (from 0 to 2π radians) indicates each time of a day (from 0 to 24 hours). For the first learning stage, the complex values are:

$$P = P_m \exp(\frac{j2\pi d}{24*60*60/res}) \tag{19}$$

$$\theta = \theta_m \exp(\frac{j2\pi d}{24*60*60/res}) \tag{20}$$

Similarly, for the second learning stage:

$$Q = Q_m \exp(\frac{j2\pi d}{24*60*60/res}) \tag{21}$$

$$V = V_m \exp(\frac{j2\pi d}{24*60*60/res}) \tag{22}$$

where $1 \leq d \leq (24*60*60/res)$ and *res* is the resolution of the real data (second). P_m, Q_m, V_m, and θ_m are the amplitudes of the real values of the active powers, reactive powers, voltage amplitudes, and angles, respectively. In this study, *res* is 4 seconds because the real data is available for this time step, based on the outputs of supervisory control and data acquisition (SCADA). The values of the voltage amplitudes and angles (V_m and θ_m) are obtained from TDPF using PSAT software. The quality of learning process depends on sampling number from input data to learn the network. With smaller sampling numbers forecasting is more accurate, but more time consuming. In this study, the sampling number is 10, which is a logical trade-off between accuracy and calculation's speed.
        Fig. 4 shows an algorithm including steps of the proposed method and comparison between forecast results and actual values in contingencies. The first phase of Fig. 4 contains steps of Fig. 3 and both TDPF and CVNN are

used. In the second phase, only TDPF is used to compare the forecast results with actual data. The actual data is TDPF's output. One of the advantages of this type of prediction is to estimate the grid behavior in the contingencies. In this paper, the proposed method has been applied to two real-world case studies to ensure the forecast results are accurate and reliable in the contingencies. The simulated contingencies in this study are: sudden loss of wind generations, changing the wind generations (based on real meteorological data of region), and loss of other generators as a fault.

V. Application of the Proposed Method

In this section two important usages of the proposed method have been described. The first one is to help the grid to adapt with the contingencies with the most efficient response. Another usage of the proposed method is to find the optimal location(s) and capacity of Battery Energy Storage Systems (BESS) in order to regulate the frequency and voltage of grid during contingencies. Following subsections describe more details.

A. Coping with the contingencies

In this study, several standard factors are used in order to ensure the accuracy of the forecast parameters. These forecast values can be utilized for various purposes. An important utilization of the forecast voltage amplitudes and angles is to adapt the grid in order to have the best reaction against the contingencies and faults. Adapting the grid means changing the power injections at generation or load buses in order to cope with contingencies successfully. The proposed heuristic method makes the grid smarter especially in the contingencies through increasing reliability, minimizing power interruption, and improving self-healing levels.

Fig. 5 shows three steps for application of the proposed method. The first part is calculation of differences between outputs of TDPF in the normal situation (without contingency) and the outputs of CVNN in contingency (as accurate forecasts). These differences are ΔV and $\Delta \theta$ in the algorithm of Fig. 5. During a contingency, the sensitive buses (generators or loads) can be detected using a sensitivity analysis because these buses have the maximum sensitivity in contingency. Two thresholds can be defined such as $\varepsilon 1$ and $\varepsilon 2$. If $\Delta V_i > \varepsilon 1$ and (or) $\Delta \theta_i > \varepsilon 2$, the ith bus is sensitive, where i is the number of the bus. The second part is to adapt the grid with calculation of ΔP and ΔQ, using equation (7). In this part, only the arrays of Jacobian matrix should be renewed which are related to the sensitive buses. The output of this part calculates values of ΔP and ΔQ for the sensitive buses. These values indicate the amounts of power which the sensitive buses (generators or loads) should generate or absorb. This adaptation leads to cope with the abnormal situations successfully with minimum interruption. Obviously, these changes (power increasing or decreasing) are based on the possible ranges of the powers in the generators and loads. The third part of the algorithm is to run a TDPF using the adapted grid to ensure about the effectiveness of the proposed method in the contingencies.

Clearly, in the contingencies, applying the proposed method helps the grid to adapt with the abnormal conditions to cope with them efficiently. Also, it avoids running time-consuming TDPF and enormous calculations of the big Jacobian matrix in the abnormal situations where timing is important. Additionally, using the heuristic method helps the operators to make the most optimized and fast decision in any contingency to maintain the grid more reliable. Fig. 6 briefly indicates the steps of the application of the proposed method. The generators (or loads) adjust their power generation (or consumption), based on the calculated values, to have the best reaction against the contingency to cope with the abnormal situation with the highest reliability.
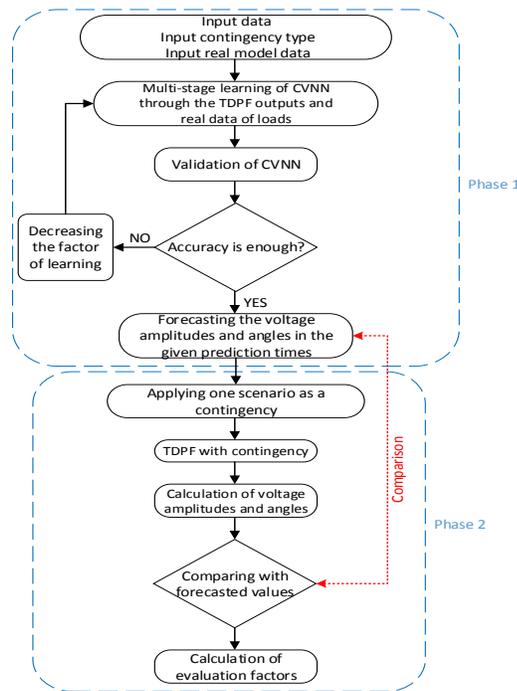
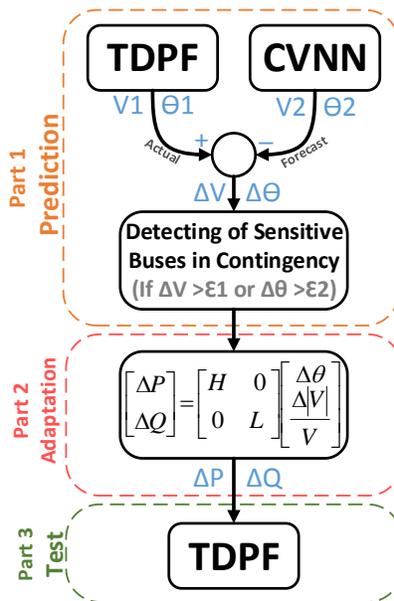Fig. 4. Two phases of algorithm of the proposed method

Fig. 5. Algorithm for the application of the proposed method

B. Finding optimal place and size of BESS

Frequency regulation needs to be done during the contingencies in the grid. For this, the optimal locations and capacities of BESS need to be determined. CVNN, TDPF, and Economic Dispatch(ED) are the tools that are used in this section for determining the locations and capacity amounts of BESS in the grid. Fig.7 shows that this process can be classified into four steps:
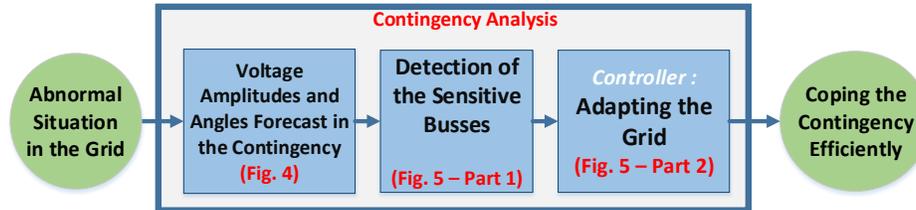

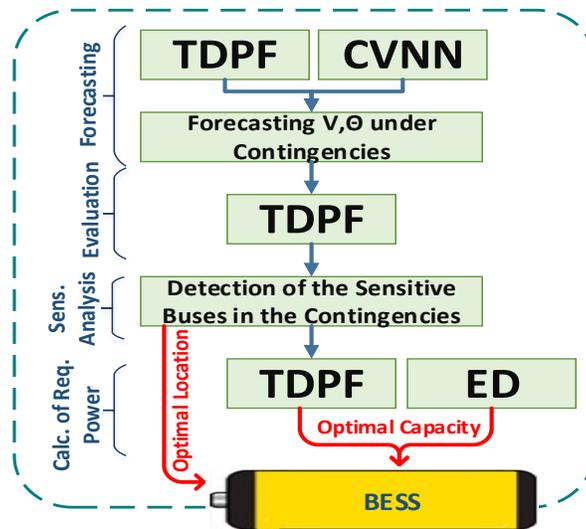Fig. 6. Contingency analysis using the proposed method

Fig. 7. Algorithm of finding optimal location and capacity of the BESS

1) *Forecasting*: This step combines CVNN and TDPF in order to forecast voltage amplitudes and angles using load data under different contingencies.
2) *Evaluation*: The purpose of this step is to ensure the accuracy of the forecasting step using an off-line process. This step compares the forecast values with actual data.
3) *Sens. Analysis*: This step applies a sensitivity analysis based on forecast results to detect the sensitive buses.
4) *Calc. of Req. Power*: This step calculates the required power using TDPF and ED for the optimal locations which has been detected in previous step.

Voltage amplitudes and angles are appropriate parameters for detecting the sensitive buses since these variables experience considerable variations during contingencies and affect the grid frequency. These sensitive buses show

highest variations regarding the mentioned parameters in the event of contingencies. By injecting the power into the grid using these sensitive locations, the grid frequency can be regulated optimally. In order to detect these buses a wide range of contingencies, including the worst case one, should be applied. This study applies losing thermal/wind generation lost and sudden/gradual change in the wind generation contingencies. The results in this paper shows, as it is accepted technically, some of the detected sensitive buses located close to the wind generation units. The required power is the amount that should be injected into the grid through the sensitive locations for frequency regulation and power shortage compensation in the worst case contingency.

VI. Case Studies

　　The proposed method has been applied to two case studies. The first one is the standard IEEE 14-bus model and the second one is a real-world model of an island in the United States (island of Maui in Hawaii). The island's grid includes 184 bus, 20 generators, and two wind farms. This case study is modeled using real data of grid's equipment, loads, and generators. Maui's generators inject power into the grid, based on a unit commitment program demonstrating priority of power production. These priorities have been considered in the modeling of Maui grid. In the unit commitment, wind turbines have the highest priority in generation. This case study simulation has been done for the peak-load time and the supposed value of spinning reserve is 10% of total capacity.

　　The applied contingency to the IEEE 14-bus model is to change the load during specific time periods when the Static Synchronous Compensator (STATCOM) is enabled. The contingencies of the second case study are three different scenarios including gradual and sudden changing of the wind generations and loss of various thermal generators. Fig. 7 illustrates the simulated model of the first case study.
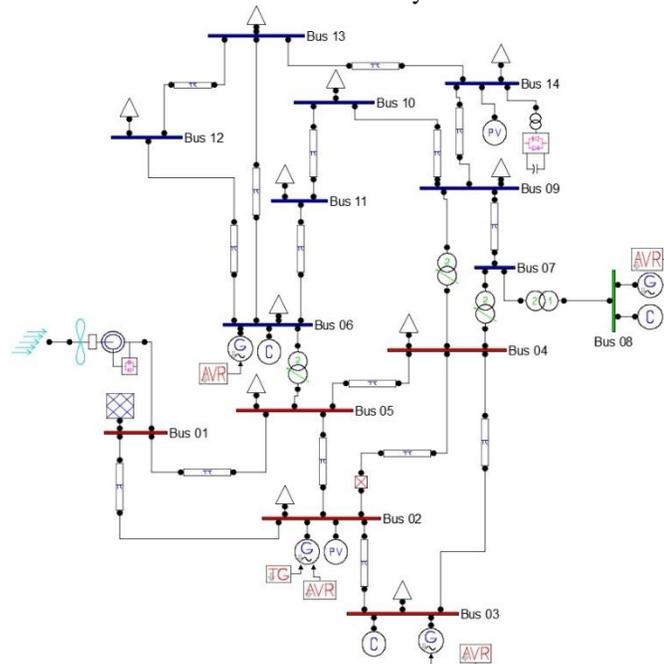

Fig. 8. The first case study: IEEE 14-bus model

After applying the proposed method to both case studies, the performance level of the forecasting is evaluated using three standard parameters including: the normalized root mean squared error (nRMSE), the coefficient of determination (R^2), and the mean absolute error (MAE). The following equations show these parameters:

$$nRMSE = \frac{\sqrt{\frac{1}{N}\sum_{k=1}^{N}|y_k - \hat{y}_k|^2}}{\bar{y}}, R^2 = 1 - \frac{\sum_{k=1}^{N}|y_k - \hat{y}_k|^2}{\sum_{k=1}^{N}|y_k - \bar{y}|^2}, MAE = \frac{\sum_{k=1}^{N}|y_k - \hat{y}_k|}{N} \qquad (23)$$

Where y and $\hat{y}$ are the actual and forecast values, respectively. $\bar{y}$ is the mean of the actual values, and N is the number of the output nodes of CVNN [28].

VI.   Results

This section includes the results of applying the heuristic method to both case studies in different scenarios of contingencies. In the first case study, the first usage of the proposed method (coping with the contingencies) has been considered, but in the second case study both usages (coping with the contingencies and finding optimal place and size of BESS) have been discussed.

A.   Case study 1

In the IEEE 14-bus model, the total time of TDPF is 20 seconds and each time step is 0.139 second. The system is learned by CVNN in the normal conditions (without contingency). A contingency has been applied to the model between 4.5 and 5.5 seconds. This contingency includes: changing the grid load (5% decreasing) and enabling STATCOM in the 14th bus. Fig. 9 demonstrates the predicted and actual values of the voltage amplitudes for all 14 buses. Actual values are the outputs of TDPF using PSAT software. Table I shows the evaluation parameters in three different times for the first case study. These results prove the high accuracy of the forecasting using the proposed method during the contingency.
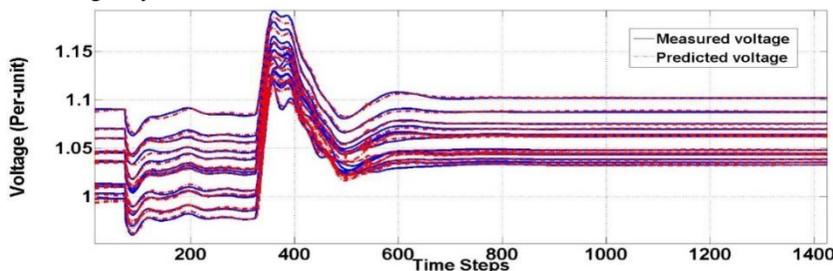

Fig. 9. The measured and predicted values of the voltage amplitudes in 14 buses of the first case study

Table I: The forecast evaluation parameters for three different times after the contingency in the first case study

Prediction Time	nRSME (%)	R2 (%)	MAE (%)
t=6.5 Sec. (1 Sec. ahead)	4.13	99.99	0.00054
t=10.5 Sec. (5 Sec. ahead)	0.03	99.99	4.4844e-08
t=15.5 Sec. (10 Sec. ahead)	0.001	99.99	5.0072e-11

B.   Case study 2

1)First Usage Results; Contingency Coping: In the real-world model of the island, real data for whole times of a day is available. In this case study, 24 hours of a day have been divided into 144 intervals of 10-minute. Each time

step of TDPF is 0.1 second. The resolution of the real data is 4 seconds. Thus, the minimum required numbers for learning through CVNN is 40, based on Equation (18). The sampling number of the learning is 10 which is a good trade-off between the accuracy and speed. Fig. 10 shows the average of the load (MW) in Maui grid in one day. The horizontal axes represents 4-second time intervals of one day, which is 21600 numbers. In this case study, one 10-minute interval has been chosen to simulate. This time is a critical one because the load goes under considerable changes. After multi-stage learning and validation, three different contingencies have been applied during this time interval.

Fig. 11 demonstrates the first scenario as a contingency, which is sudden loss of both wind generations from their maximum output to zero. The number of time steps are 6000 because the total time of TDPF is 10 minutes and each time step is 0.1 second. The values of vertical axes are per-unit with the base power of 100 MVA. With decreasing the wind generations, other generators inject the power into the grid, based on their priority (unit commitment program). Different colors of Fig. 11 show the outputs of different generators. The second scenario is to change the wind generations, based on the meteorological data of Maui, which has been shown in Fig. 12. This figure demonstrates changes of the wind generations in one hour (3600 seconds) of a day. The third scenario is loss of the other generations in some special times of TDPF, which Fig. 13 represents it. Each color demonstrates output of one generator which is zero in special times. During the time domain simulation, dynamic parameters such as eigenvalues have been controlled to ensure the grid operates in the stable zone.
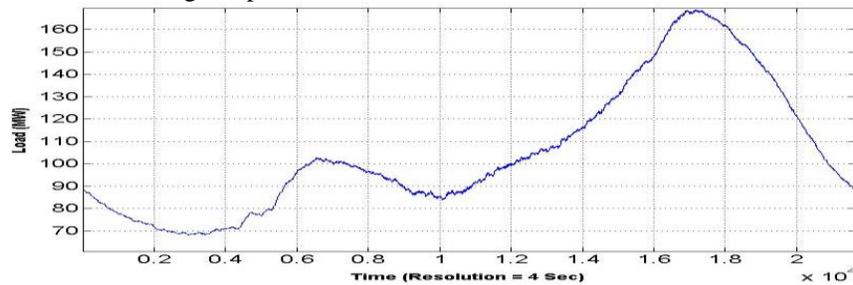

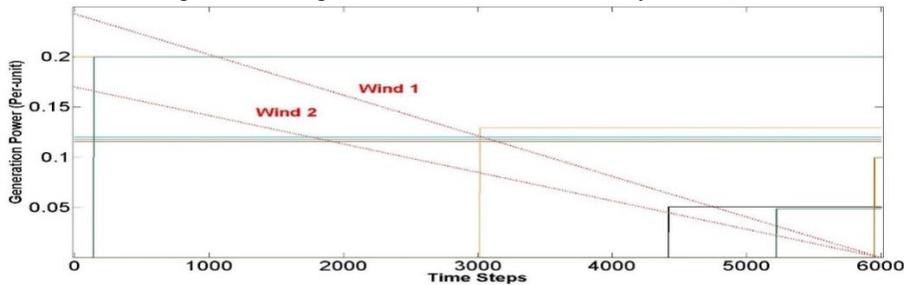Fig. 10. Average of the load (MW) in one day of Maui

Fig. 11. Scenario 1 - Decreasing the wind outputs from maximum to zero

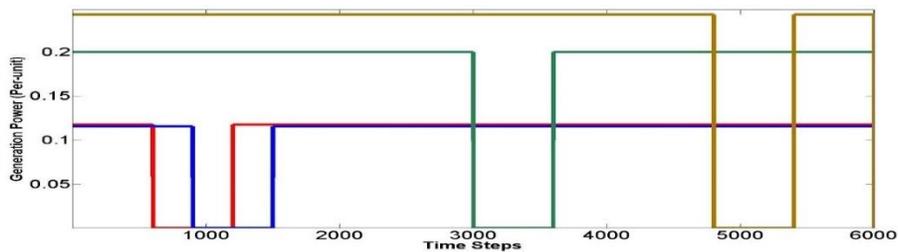Fig. 12. Scenario 2 - Changing the wind generations in one hour of a day

Fig. 13. Scenario 3 - Loss of the other generations in different times of TDPF

Fig. 14 shows the percentage of differences between the forecast (CVNN) and the actual values (TDPF) of the voltage amplitudes in all buses of the second case study. The first two curves are related to time $t = 590$ second of TDPF which is a critical time. In the third scenario, the chosen prediction time is another critical time which is the time of loss of a big generator ($t = 490$ second). The values of horizontal axes are the bus numbers. Fig. 15 illustrates both forecast and actual values of the voltage angles for the second case study. The chosen prediction times are the same as Fig. 11. The results of Fig. 14 and 15 prove the high accuracy of the heuristic method to forecast the voltage amplitudes and angles in the contingencies.
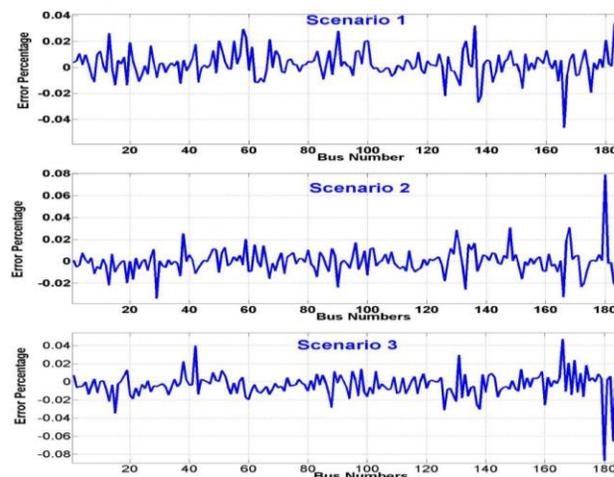

Fig. 14. Error between the forecast and actual voltage amplitudes (in $t = 590$ Sec. for the 1st and 2nd Scenarios and $t = 490$ Sec. for the 3rd scenario)

Table II shows the evaluation parameters of prediction for the voltage amplitudes in the second case study. In this table, the chosen prediction times are several critical times in TDPF. The same information for the voltage angles has been demonstrated in Table III. These results prove the good performance of the proposed method in the forecasting in the contingencies.
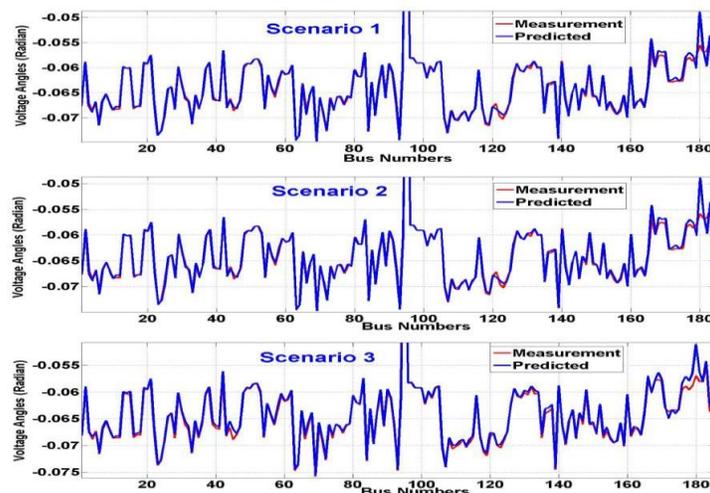
Fig. 15. Forecast and actual voltage angles (in time of t = 590 Sec: for the 1st and 2nd Scenarios and t = 490 Sec: for the 3rd scenario)

Table II: Forecast evaluation parameters of voltage amplitudes in critical times of the scenarios (second case study)

Contingency	Time(Sec.)	nRSME(%)	R2(%)	MAE(%)
	t=590	0.048	99.99	1.27e-6
Scenario 1	t=390	0.075	99.99	3.04e-6
	t=180.1	0.060	99.997	1.94e-6
	t=590	0.052	99.99	1.48e-6
Scenario 2	t=390	0.076	99.995	3.15e-6
	t=180.1	0.046	99.998	1.14e-6
	t=70	0.060	99.997	1.95e-6
Scenario 3	t=305	0.074	99.995	2.93e-6
	t=590	0.064	99.995	2.21e-6

Table III: Forecast evaluation parameters of voltage angles in some critical times of the scenarios (2nd case study)

Contingency	Time(Sec.)	nRSME(%)	R2(%)	MAE(%)
	t=590	0.916	99.99	4.68e-5
Scenario 1	t=390	1.632	99.992	1.52e-4
	t=180.1	0.795	99.998	3.63e-5
	t=590	0.947	99.997	5.01e-6
Scenario 2	t=390	1.638	99.992	1.53e-4
	t=180.1	0.731	99.998	3.06e-5
	t=70	0.896	99.997	4.613e-5
Scenario 3	t=305	2.100	99.987	2.52e-4
	t=590	0.896	99.997	4.61e-5

2) Second Usage Results: Optimal Location and Capacity of BESS: As it was depicted in Fig.7, after evaluating the forecasted parameters, a sensitivity analysis should be performed in order to find the optimum buses for the storage system. In this part a wide range of contingencies, as it was shown in Fig.11 to 14, are applied in order to find these optimum places. Fig.16 shows the results for sensitivity analysis. Bus numbers 166 and 180, based on this figure, show the maximum sensitivity during different contingencies. This means that these buses are the optimum locations for the BESS. Bus 180 is a generator bus and using the storage system for this bus has two advantages: frequency regulation in the abnormal conditions and compensating the power shortage in the contingencies in order to have the

minimum power interruption. Bus 166, on the other hand, is a load bus which is an appropriate bus for installing batteries in order to decrease fluctuations related to distribution side.

Next step is calculating the capacity for these storage systems. For this the worst case scenario should be considered which is losing the largest generation unit. This amount is 24.3 MW for Maui grid. Based on equation (7) and performing TDPF, for the Maui grid, 15.73 MW power should be injected through the sensitive buses in order to regulate the frequency and compensate the power shortage. Determining the BESS capacity should be done through ED based on minimizing the cost function of available generators and batteries. Table IV shows the optimal output of power sources for generators and BESS. These amount has been calculated at the lowest cost considering both transmission and operational constraints. As it is shown it the table, BESS should be allocated in bus 180 (sensitive generation bus) with the capacity of 0.93 MW. Considering the minimum and maximum for State Of Charge (SOC) of batteries, in order to maximize lifetime and efficiency, the active power of the transmission part of the BESS can be calculated as:

$$0.93MW * \frac{1}{SOCmax - SOCmin} = 0.93MW * \frac{1}{0.8 - 0.2} = 1.55MW \tag{24}$$

Based on historical data, the maximum time for the contingency in Maui is one hour. Considering this amount, BESS should supply 1.55 MWhr to cope with this condition and regulate the frequency in the grid. The simulation results for Maui shows that, based on the proposed method, 1.55MWhr should be provided by BESS in bus 180 in order to cope the contingency in this island.
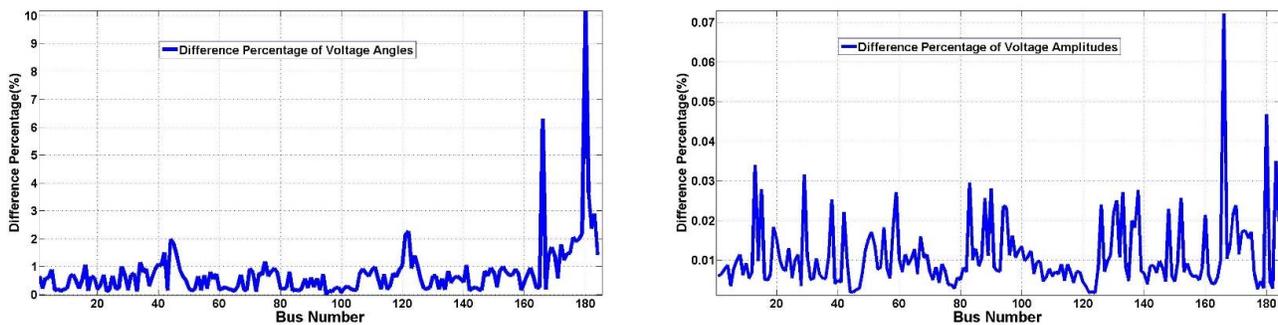

Fig. 16. Results of the sensitivity analysis for the voltage amplitudes and angles in a wide range of contingencies

Table IV; ED results: optimal outputs of the available generators and BESS to cope with the worst case of contingency and regulate the frequency

Power Source	Generation Power (MW) (based on ED results)
Gen. bus 48	1.8
Gen. bus 49	2.2
Gen. bus 50	3.3
Gen. bus 53	2.8
Gen. bus 140	2.2
Gen. bus 181	2.5
BESS bus 180	**0.93**

VIII. Conclusion

Increasing the ability of power grid to cope with contingencies, can significantly improve the grid reliability. In this paper, we proposed a heuristic forecast method to predict the voltage amplitudes and angles in the power grid. This method is a combination of multi-stage learning of CVNN and TDPF. One important applications of these forecast values is to adapt the grid to have the best reaction against the contingencies and faults. Adapting the grid means changing the power injection or absorption at generation or load buses. Using the proposed method helps to cope with the contingencies with highest reliability and efficiency and lowest cost and power interruption. With applying the heuristic method, not only the grid can work smarter, but also reliability of the grid can be increased,

especially in the contingencies. Additionally, using this method avoids enormous and time consuming power flow calculations in the abnormal situations. Another important usage of the proposed method is to obtain the optimal location(s) and capacity of the storage system in order to manage the contingencies and regulate the frequency and voltage.

References

[1] H. Sangrody, M. Sarailoo, N. Zhou, N. Tran, M. Motalleb, and E. Foruzan, "Weather forecasting error in solar energy forecasting," IET Renewable Power Generation, 2017.

[2] P. S. Paretkar, L. Mili, V. Centeno, K. Jin, and C. Miller, "Short-term forecasting of power flows over major transmission interties: Using Box and Jenkins ARIMA methodology," in Power and Energy Society General Meeting. IEEE, Jul. 2010.

[3] C. Xie, W. Liu, J. Wen, and J. Wang, "An Auto-Generated Method of Day-Ahead Forecast Powerflow for Security Correction of Power Grid Maintenance Scheduling," in Engineering Conference (APPEEC), Asia-Pacific. IEEE, Mar. 2012.

[4] Z. Bing-da and G. Hong-wu, "The Control Strategy for Optimization of Voltage and Reactive Power in Substation Based on Load Forecasting," in Spring Congress on Engineering and Technology (S-CET). IEEE, May 2012.

[5] X. Liu and H. Wang, "Area automatic voltage control based on wind power forecasting of large-scale wind farms," in Innovative Smart Grid Technologies - Asia (ISGT Asia). IEEE, May 2012.

[6] Z. Zhou, A. Botterud, J. Wang, R. Bessa, H. Keko, J. Sumaili, and V. Miranda, "Application of probabilistic wind power forecasting in electricity markets," Wind Energy, vol. 16, no. 3, pp. 321–338, Apr. 2013.

[7] A. Botterud, ZhiZho, J. Wang, J. Sumaili, H. Keko, J. Mendes, R. J. Bessa, and V. Miranda, "Demand dispatch and probabilistic wind power forecasting in unit commitment and economic dispatch: A case study of illinois," IEEE Transactions on Sustainable Energy, vol. 4, no. 1, pp. 250–261, Jan. 2013.

[8] F. Dragomir and O. E. Dragomir, "Distributed Power Generation from Renewable Energy Resources: A Framework for Load Forecasting in Low Voltage Power Grids," in Sixth UKSim/AMSS European Symposium on Computer Modeling and Simulation (EMS). IEEE, Nov. 2012.

[9] W. Hoiles and V. Krishnamurthy, "Nonparametric demand forecasting and detection of energy aware consumers," IEEE Transactions on Smart Grid, vol. 6, no. 2, pp. 695–704, Mar. 2015.

[10] W. Heins, N. Ell, H. P. Beck, and C. Bohn, "State observation in medium-voltage grids with incomplete measurement infrastructure through online correction of power forecasts," in European Control Conference(ECC). IEEE, Jun. 2014.

[11] S. Anbazhagan and N. Kumarappan, "Day-ahead deregulated electricity market price forecasting using recurrent neural network," IEEE Systems Journal, vol. 7, no. 4, pp. 866–872, Dec. 2013.

[12] R. de Aquino, H. Gouveia, M. Lira, A. Ferreira, O. Neto, and M. Carvalho, "Wind forecasting and wind power generation: Looking for the best model based on artificial intelligence," in The International Joint Conference on Neural Networks (IJCNN). IEEE, Jun. 2012.

[13] R. J. Bessa, V. Miranda, A. Botterud, J. Wang, and E. M. Constantinescu, "Time adaptive conditional kernel density estimation for wind power forecasting," IEEE Transactions on Sustainable Energy, vol. 3, no. 4, pp. 660–669, Oct. 2012.

[14] H. Quan, D. Srinivasan, and A. Khosravi, "Short-term load and wind power forecasting using neural network-based prediction intervals," IEEE Transactions on Neural Networks and Learning Systems, vol. 25, no. 2, pp. 303–315, Feb. 2014.

[15] A. Yona, T. Senjyu, T. Funabashi, and C.-H. Kim, "Determination method of insolation prediction with fuzzy and applying neural network for long-term ahead pv power output correction," IEEE Transactions on Sustainable Energy, vol. 4, no. 2, pp. 527–533, 2013.

[16] V. Kurbatsky, N. Tomin, D. Sidorov, and V. Spiryaev, "Application of two stages adaptive neural network approach for short-term forecast of electric power systems," in 10th Environment and Electrical Engineering International Conference(EEEIC). IEEE, 2011.

[17] D. Lee and R. Baldick, "Short-term wind power ensemble prediction based on gaussian processes and neural networks," IEEE Transactions on Smart Grid, vol. 5, no. 1, pp. 501–510, Jan. 2014.

[18] M. Rejc and M. Pantos, "Short-term transmission-loss forecast for the slovenian transmission power system based on a fuzzy-logic decision approach," IEEE Transactions on Power Systems, vol. 26, no. 3, pp. 1511–1521, Aug. 2011.

[19] V. Kurbatsky, N. Tomin, D. Sidorov, and V. Spiryaev, "Hybrid genetic algorithms for forecasting power systems state variables," in IEEE Grenoble PowerTech. IEEE, Jun. 2013.

[20] D. Saez, F. Avila, D. Olivares, C. Canizares, and L. Marin, "Fuzzy prediction interval models for forecasting renewable resources and loads in microgrids," IEEE Transactions on Smart Grid, vol. 6, no. 2, pp. 548–556, Mar. 2015.

[21] D. V. M. Chary and J. Amarnath, "Power system contingency analysis using complex valued neural networks," International Journal of Applied Engineering Research, vol. 4, no. 9, p. 1789, 2009.

[22] A. Keyhani, Design of Smart Power Grid Renewable Energy Systems. Wiley-IEEE Press, 2011.

[23] F. Milano, Power System Analysis Toolbox, Documentation for PSAT, User's Manual, 2008.

[24] K. E. Brenan, S. L. Campbell, and L. R. Petzold, Numerical Solution of Initial-Value Problems in Differential-Algebraic Equations. Society for Industrial and Applied Mathematics, 1995.

[25] M. Motalleb, M. Thornton, E. Reihani, and R. Ghorbani, "A nascent market for contingency reserve services using demand response," Applied Energy, vol. 179, pp. 985–995, 2016.

[26] M. Motalleb, M. Thornton, E. Reihani, and R. Ghorbani, "Providing frequency regulation reserve services using demand response scheduling," Energy Conversion and Management, vol. 124, pp. 439–452, 2016.

[27] A. Hirose, Complex-Valued Neural Networks: Advances and Applications. IEEE Press Series on Computational Intelligence, 2013.

[28] L. S. Saoud, F. Rahmoune, V. Tourtchine, and K. Baddari, "Complex-valued forecasting of the global solar irradiation," Journal of Renewable and Sustainable Energy, vol. 5, pp. 043 124:1–21, Aug. 2013.

[29] E. Reihani, M. Motalleb, R. Ghorbani, and L. S. Saoud, "Load peak shaving and power smoothing of a distribution grid with high renewable energy penetration," Renewable Energy, vol. 86, pp. 1372–1379, 2016.

[30] M. Motalleb, E. Reihani, and R. Ghorbani, "Optimal placement and sizing of the storage supporting transmission and distribution networks," Renewable Energy, vol. 94, pp. 651–659, 2016.